Energy 193 (2020) 116658

Contents lists available at ScienceDirect

Energy

journal homepage: www.elsevier.com/locate/energy

Experimental and numerical investigation on hydrothermal performance of nanofluids in micro-tubes

M. Behi [a, b, *], M. Shakorian-poor [c], S.A. Mirmohammadi [b, d], H. Behi [e, i], J.I. Rubio [b], N. Nikkam [f], M. Farzaneh-Gord [g], Y. Gan [d], M. Behnia [h]

[a] School of Chemical and Biomolecular Engineering, The University of Sydney, Sydney, NSW, 2006, Australia
[b] Department of Energy Technology, KTH Royal Institute of Technology, SE-10044, Stockholm, Sweden
[c] The Faculty of Mechanical Engineering, Shahrood University of Technology, Shahrood, Iran
[d] School of Civil Engineering, The University of Sydney, Sydney, NSW, 2006, Australia
[e] Research Group MOBI – Mobility, Logistics, and Automotive Technology Research Centre, Vrije Universiteit Brussel, Pleinlaan 2, Brussels, 1050, Belgium
[f] Faculty of Life Sciences and Biotechnology, Shahid Beheshti University, Tehran, Iran
[g] Faculty of Engineering, Mechanical Engineering Department, Ferdowsi University of Mashhad, Mashhad, Iran
[h] School of Management, Macquarie University, Sydney, Australia
[i] Flanders Make, Heverlee, 3001, Belgium

ARTICLE INFO

Article history:
Received 26 March 2019
Received in revised form
7 November 2019
Accepted 28 November 2019
Available online 3 December 2019

Keywords:
Nanofluids
Nanoparticles
Laminar flow
Micro-tube
Modeling
Heat transfer coefficient
Friction factor

ABSTRACT

Nanoscale solid particles suspended in a base liquid are a new class of nano-engineered colloidal suspension, defined with a coined name of nanofluids (NFs). The effect of dispersing nanoparticles (NPs) on the hydraulic and thermal (hydrothermal) performance of the conventional coolants is a matter of importance in many applications. This work experimentally and numerically presents the effect of different parameters, including the concentration and size of the NPs, on two primary parameters, namely heat transfer coefficient and friction factor in a microtube. The numerical modeling of colloidal suspensions was conducted based on single-phase as well as Eulerian-Mixture two-phase approaches and showed a good agreement with experimental results. The numerical results displayed that the suspended NPs remarkably increased the convective heat transfer coefficient as well as friction factor by as much as 42% and 22% (in NP concentration range of 1%–9%, and NP size range of 13–130 nm and Reynolds number of 400) respectively. Besides, two new correlations were developed based on the results obtained from experimentally validated models to predict the hydrothermal response of NFs in the laminar regime. Moreover, correlations were successfully created to predict the Nusselt number and friction factor of nanofluids, with ±8% and ±5% agreement between numerical data and predictions, respectively.

1. Introduction

Nano-engineered fluids are binary mixtures that have coexistence between two phases (solid-liquid), dispersing NPs in the base liquids. During the past decades, the transport phenomena of liquids including heat and mass transfer characteristics have been of great interest in a wide variety of applications. For instance, miniaturized systems such as nano-electromechanical systems (NEMS) technology [1] and nanofluids [2–5] have recently received considerable attention. Thermal conductivity and heat transfer coefficient serve as the most significant thermal characteristics of materials in relevant studies. Hence, many studies have been conducted in this area to explore and introduce materials with enhanced thermo-physical properties [6–8]. In one of the most recent studies, Mirmohammadi et al. have investigated the thermophysical properties of water-based silver nanofluid experimentally and using Molecular Dynamic simulation [9]. They studied the effect of particle shape, temperature, and volume concentration on the thermal conductivity and viscosity, proposing correlations for the relative thermal conductivity and relative viscosity of nanofluids.

Nanosuspensions as complex liquids (solid NPs in base liquid), namely nanofluids (NFs), with enhanced thermo-physical properties including thermal conductivity were pioneered by Choi and Eastman [10]. NFs are liquids containing nano-scale solid particles

* Corresponding author. School of Chemical and Biomolecular Engineering, The University of Sydney, Sydney, NSW, 2006, Australia.
E-mail addresses: mbehi@kth.se, m.behi@sydney.edu.au (M. Behi).

https://doi.org/10.1016/j.energy.2019.116658
0360-5442/

Nomenclature

A	area, m^2
Cc	Cunningham correction
D_T	thermophoresis coefficient
C_d	drag coefficient
C_p	specific heat capacity, J/kgK
D	pipe diameter, m
d_p	nanoparticle diameter, m
F	friction factor,
H	heat transfer coefficient, W/m^2 K
h_v	volumetric heat transfer coefficient, W/m^2K
K	thermal conductivity, W/m K
K_B	Boltzmann constant, J/K
L	length, m
x^*	Dimensionless length, $(L/D_{in})/(RePr)$
$\dot{m}$	mass flow rate, kg/s
Nu	Nusselt number, $h D_{in}/k$
Pr	Prandtl number, $(C_p \mu)/k$
Pe	particle Peclet number, $(ud_p)/\alpha_{nf}$
Re	Reynolds number, $(\rho u_m D_i)/\mu$
ΔP	pressure drop, Pa
q''	heat flux, W/m^2
P	pumping power, W
Q	heat, W
F_{col}	Particle-particle interaction force, N/m^3
F_d	drag force, N/m^3
F_{mv}	virtual mass force, N/m^3
F_T	thermophoresis force, N/m^3
F_B	brownian force, N/m^3
T	temperature, C
U	velocity, m/s
V_T	thermophoretic velocity, m/s
X	axial distance, m
$\dot{\forall}$	volume flow rate, m^3/s

Greek letters

ϕ	volume fraction
λ	mean free path, m
ξ	Gaussian random number
μ	Dynamic viscosity, Pa.s
ν	Kinematic viscosity, m^2/s
β	friction coefficient, kg/m^3s
ρ	density, kg/m^3

Subscript

eff	Effective
Ave	Average
col	collision of particles
Bl	base liquid
Eff	Effective
Nf	Nanofluid
F	Fluid
In	Inner
Out	Outer
P	Nanoparticle
S- in	surface-inner
S- out	surface-outer

Abbreviations

NF	Nanofluid
TC	Thermal Conductivity
W/EG	water/ethylene glycol mixture
HTC	NP Heat Transfer Coefficient Nanoparticle

that are typically smaller than 100 nm. The interaction between dispersed solid NPs with each other and/or with liquid causes increases in heat transfer performance of the coolant. As an example, Eastman et al. [11] reported that a small quantity of Cu NPs in ethylene glycol (EG) could increase the thermal conductivity by about 40%. Since then, many researchers used NFs as a coolant in a vast number of applications such as cooling of electronics, transport vehicles, data centers, power generation devices, etc. [12–14].

For many industries, laminar convective heat transfer is essential for heating, and cooling purposes since the turbulent flow cannot be used in compact heat exchangers [15,16]. Besides, numerous applications need high heat flux cooling micro-channels in which the addition of nanoparticle to the base liquid (nanofluids) can be a solution [17,18]. Many studies in the literature are focusing on this area and reporting that dispersing a small quantity of solid NPs may improve the thermal conductivity and convective heat transfer performance of the conventional fluids [19–21]. In line with studying the thermal properties of the NFs, many researchers have also investigated the effect of the addition of NPs on pressure drop in different systems. Hwang et al. [22] investigated on pressure drop and heat transfer performance using water-based Al_2O_3 NFs. They observed 8% increase in heat transfer coefficient for NF containing 0.3% volume Al_2O_3 NPs. Moreover, their experimental results for friction factor showed a good agreement compared to the theoretical results obtained from the relevant correlation for the single-phase flow [22].

Several studies have been carried out to evaluate the performance of NFs in micro-sized channels during the past decades. Hojati et al. [23] investigated the forced convection of NFs in a microtube under the constant temperature boundary condition, and their results exhibited that NFs have a higher heat transfer coefficient and Nusselt number compared to the base liquid. An experimental study by Haghighi et al. [24] displayed that the Nusselt (Nu) number at any given Reynolds (Re) number increases up to ~30% for water-Al_2O_3 and water-ZrO_2 NFs, and by around 10% for water-TiO_2. Cooling of electronics using NFs was studied by Nguyen et al. [25], and based on their results, the heat transfer coefficient could be increased by up to 40%. In a numerical study on laminar flow in the microchannel by Koo and Kleinstreuer [26], it has been presented that NFs with higher thermal conductivity and channels with higher aspect ratio lead to better performance in convective heat transfer. This sort of experiment was conducted on both single-phase and two-phase heat transfer. In combined research by Lee and Mudawar [27] effectiveness of NFs in both phases has been investigated and presented that NPs have a considerable impact on thermal boundary layer development. Recently, a numerical study on copper/water NFs a microchannel Ganesan et al. [28] was carried out. They observed that the two-phase model is found to be relatively less accurate than the single-phase model. Effect of viscous dissipations has been investigated on the thermal performance of microchannel with an analytical study by Hung, and it has been observed that thermal performance is overrated when the viscous dissipation is neglected [29]. Lelea and Nisulescu [30] accomplished research on laminar nanofluid heat transfer in micro-tubes considering the viscous dissipation effect, and they concluded that heat transfer is continuously increasing with the axial distance which is a different mechanism compared to macroscale heat transfer. Developing new correlations to predict the heat transfer and fluid flow behavior of

NFs has been reported in previous studies. For a laminar flow regime in a rectangular channel, Azizi et al. [31] developed a new correlation for *Nu* number and friction factor as a function of Re number, Pr number, and concentration of the particles. In a similar a study for a circular channel by Zhang et al. [32], quite similar correlation was proposed for *Nu* number; however, based on their developed correlation the friction factor was the only function of Re number and concentration. Therefore, a change in Pr number for this type of channel does not have an impact on the friction factor. Recently, Iyahraja et al. developed two correlations for convective heat transfer and friction factor of silver-water nanofluids (0.01, 0.05, and 0.1 vol% and size of 20 nm) in a horizontal circular pipe in the laminar flow regime [33]. Also, a numerical investigation on heat transfer characteristics and friction factor of aqueous CuO nanofluids (0.005, 0.01, and 0.1% vol.) were conducted for a set of four microchannels connected in parallel under laminar regime [34].

Based on the literature review, several studies have focused on the thermophysical properties of NFs [9,35,36]. Furthermore, some investigations have been reported on the convective heat transfer of nanofluids function of nanoparticles concentrations in the laminar regime [31–34]. However, to the best knowledge of authors, minimal research [37] has been carried out to investigate the effect of both NPs loading and size simultaneously on the hydrothermal performance of NFs in microscale. The current study was aimed to fill the research gap in the convection heat transfer of nanofluids in the laminar flow regime by developing two correlations for convective heat transfer and friction factor function of NPs size and loading. In the first step, the thermophysical properties of Al_2O_3 NFs that are the crucial features of the numerical study have been carefully investigated. Thus, the two most accurate correlations capable of predicting the thermal conductivity and viscosity of NFs are employed to model NFs dynamic behavior. The effects of different parameters including volume concentration and size of NPs, and dimensionless numbers such as *Pe* number, Re number, Pr number on heat transfer coefficient and friction factor for NFs in microscale and the laminar regime are investigated. Finally, two correlations are presented to predict the hydrothermal performance of the NF.

2. Experimental study

2.1. NF preparation and experimental setup

Al_2O_3 NPs with respective sizes of around 70 nm were purchased. Al_2O_3 nanofluids containing 9 wt% of Al2O3 NPs were fabricated via a two-step method by adding a known weight of NPs in the base liquids and Ultrasonic mixing of the suspension (Chemical instruments AB, CiAB) for 30 min [38]. Finally, a series of stable Al_2O_3 nanofluids with the concentration of 9 wt% was obtained. All nanofluids were stable for at least 96 h without any visual precipitation. The volume fraction of the NFs is calculated based on the weight and density of the base liquids (ultrapure water, $\rho = 0.99821$ g/cm3) and NPs (Al_2O_3, $\rho = 3.95000$ g/cm3) at a certain temperature. The effect of temperature on the change of the weight fraction variation was neglected as the mass of the nanoparticles to the base liquid is constant. The size of Al_2O_3 NP in liquid media was measured by Dynamic Light Scattering (DLS) and the average particle size was estimated to be 223 nm.

The convective heat transfer experiment was carried out on an insulated annular stainless steel micro-tube (ID 0.50 mm with 0.15 mm thickness and 30 cm length), shown in Fig. 1. A syringe pump (Legato 200 KDS) was used to maintain the nanofluids flow in an open flow loop under the laminar flow condition. The tube was resistively heated with a DC power supply (GW Instek PSP-405) and 12 T-type thermocouples were utilized for recording the outer wall temperature distribution along the length of the tube. A thermally conductive epoxy (Omega OB-101-1/2) was used to attach the thermocouples to the test section. Moreover, two T-type thermocouples were used to record the inlet and the outlet temperatures of the test section. All thermocouples were calibrated in a reference bath at various calibrating temperatures in the 20–60 °C range and the accuracy was ±0.08 °C. To measure the pressure drop, a differential pressure transducer (GE UNIK 5000, 0–2 bar) with the accuracy ±0.032 bar was used. A digital balance, KERN FKB 16K0.05, with ±0.01 g accuracy, was used to measure the mass flow rate. The balance was connected to the computer to log the data. All the data was recorded by a data logger every 3 s, and the steady-state data were used for calculating local heat transfer coefficients.

2.2. Error analysis

Error analysis was carried out by calculating the error of each measured parameter. The uncertainty of a dependent parameter is calculated based on the uncertainty of independent variables. For instance, the uncertainty of *Nu* refers to the errors in the measurements of volume flow rate, hydraulic diameter, and all the temperatures. If parameter z is a function of several independent variables, x_i, according to the method described by Andraos [39], the overall uncertainty in z is calculated as follows:

$$\Delta z = \pm\sqrt{\sum_{i=1}^{n}\left(\frac{\partial f}{\partial x_i}\right)^2 (\Delta x_i)^2} \tag{1}$$

The uncertainties of thermocouples, the scale, and the pressure drop transducer were ±0.08 °C, of ±0.01 g ± 0.032 bar, respectively. The uncertainties for length were ±1 mm, and the diameter was ±0.01 mm. The uncertainties for average *Nu*, Re were calculated as 5.35% and 8.10% correspondingly.

3. NF and micro-tube modeling

3.1. Physical model

The two-dimensional geometric domain of a microtube with a length of 30 cm with inner diameters 0.5 mm is illustrated in Fig. 2. Flow and the thermal field are considered axisymmetric, concerning the flow physics. The NF is containing Al_2O_3 as NPs and water as the base liquid. Moreover, simulations were performed for the particle volumetric concentrations of 0–9% and NP diameters of 13–130 nm. At the inlet region, the fluid enters with uniform temperature and axial velocity profiles. The tube has an appropriate length in order to obtain a fully developed velocity and thermal profiles in the outlet region. Wall is considered to have uniform heat flux.

3.2. Mathematical modeling

3.2.1. Single-phase model

In the single-phase models, the base liquid and NPs are considered to have the same temperature and velocity field. In a homogeneous single-phase model, the conservation equations are similar to base fluid one, but thermophysical properties will be replaced with effective properties of the NFs. Dimensional conservation equations for steady-state flow are shown as followings:

Continuity equation:

$$\nabla.\left(\rho_{nf}\boldsymbol{V}\right) = 0 \tag{2}$$

Momentum equation:

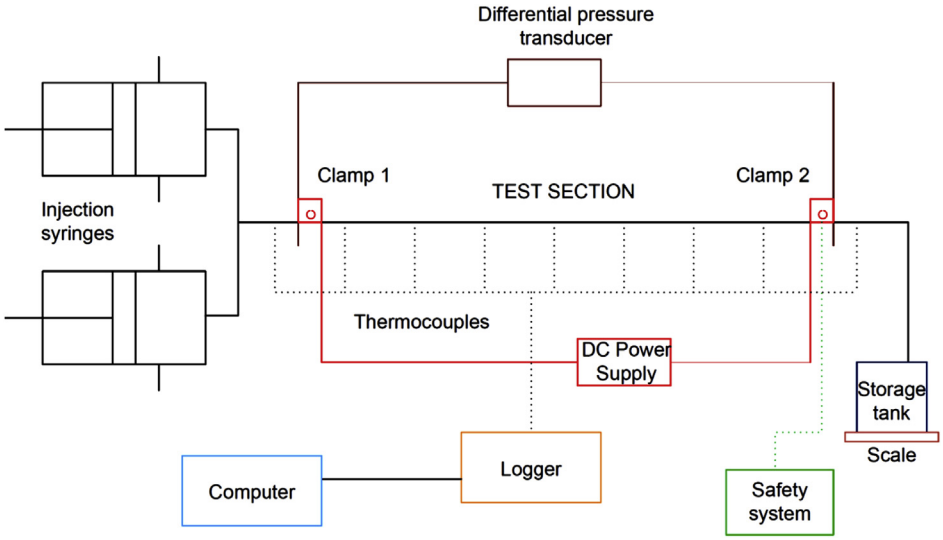

Fig. 1. Schematic of the experimental setup and microtube under study.

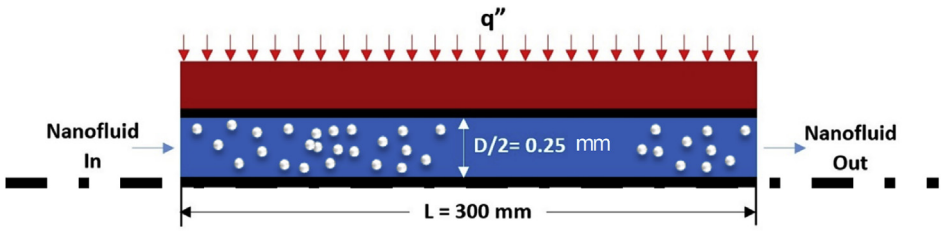

Fig. 2. Schematic of the microtube under study including the dimensions.

$$\nabla.\left(\rho_{nf}\boldsymbol{VV}\right) = -\nabla P + \nabla.\left(\mu_{nf}\nabla\boldsymbol{V}\right) \tag{3}$$

Energy equation:

$$\nabla.\left((\rho C_P)_{nf}\boldsymbol{V}T\right) = \nabla.\left(K_{nf}\nabla T\right) \tag{4}$$

wherein ρ_{nf} , μ_{nf}, K_{nf} and C_{nf} are the density, the viscosity, the thermal conductivity and the specific heat of NF, respectively.

Since the suspended particles in NFs are quite small regarding the size, it has been suggested that these particles may be readily fluidized. Consequently, by overlooking the slip motion between fluid and NPs, and the assumption of thermal equilibrium between them, much research has treated NFs as a homogenous fluid. In this approach, the conservation equations are similar to those of homogenous fluids except that the effective properties of the NF are applied for thermo-physical properties. On the one hand, this method is more straightforward than other approaches and requires less time of calculations. On the other hand, some researchers have claimed that this method provides results relatively close to the experimental ones [40].

Further details regarding the single-phase numerical solution are mentioned in the numerical methodology section.

3.2.2. Eulerian-Mixture two-phase model

In this model, slip velocity between NPs and base liquid is considered to be small, and there is a strong coupling between them. For the entire NF mixture, one momentum and one energy equation are computed, and each phase has its velocity and volume fraction in each computational cell. In the steady-state flow, governing equations consisting of mass, momentum, and energy are derived for the mixture model as follows:

Mixture continuity:

$$\nabla.(\rho_m\boldsymbol{V_m}) = 0 \tag{5}$$

Mixture conservation of momentum:

$$\nabla.(\rho_m\boldsymbol{V_m}\boldsymbol{V_m}) = -\nabla P_m + \nabla.\left[\mu_m\left(\nabla\boldsymbol{V_m} + \nabla\boldsymbol{V_m^T}\right)\right] + \rho_m\boldsymbol{g} - \nabla.\sum_{k=1}^{2}\varphi_k\rho_k\boldsymbol{V_{dr,k}}\boldsymbol{V_{dr,k}} \tag{6}$$

where V_m and ϕ are mixture velocity and volume fraction, respectively. The drift velocity is defined as:

$$\boldsymbol{V_{dr,k}} = \boldsymbol{V_k} - \boldsymbol{V_m} \tag{7}$$

$$\boldsymbol{V_m} = \frac{\rho_P\varphi_P\boldsymbol{V_P} + \rho_{bf}\varphi_{bf}\boldsymbol{V_{bf}}}{\rho_m} \tag{8}$$

$$\rho_m = \rho_P\varphi_P + \rho_{bf}\varphi_{bf} \tag{9}$$

The velocity of the particles relative to the base liquid, known as slip velocity, is defined as below:

$$\boldsymbol{V_{bf,P}} = \boldsymbol{V_{bf}} - \boldsymbol{V_P} \tag{10}$$

The relation between drift velocity and slip or relative velocity is:

$$\boldsymbol{V}_{\mathbf{dr,P}} = \boldsymbol{V}_{\mathbf{P,bf}} - \left(\frac{\rho_P \varphi_P}{\rho_m}\boldsymbol{V}_{\mathbf{P,bf}}\right) = \frac{\rho_{bf}\varphi_{bf}}{\rho_m}\boldsymbol{V}_{\mathbf{bf,f}} \tag{11}$$

The slip velocity can be calculated from the following algebraic equation proposed by Manninen et al. [41]:

$$\boldsymbol{V}_{\mathbf{bf,P}} = \frac{\rho_P d_P^2}{18\mu_{bf} f_d}\frac{(\rho_P - \rho_m)}{\rho_P}\left[\boldsymbol{g} - (\boldsymbol{V}_{\mathbf{m}}.\nabla)\boldsymbol{V}_{\mathbf{m}} - \frac{\partial \boldsymbol{V}}{\partial t}\right] \tag{12}$$

The drag function f_d can be obtained from Schiller and Naumann [38] drag formulation as below:

$$f_d = \begin{cases} 1 + 0.15Re_P^{0.687} & Re_P \le 1000 \\ 0.0183Re_P & Re_P > 1000 \end{cases} \tag{13}$$

The particle Reynolds number (Re_p) is defined as:

$$Re_P = \frac{d_P \rho_{bf} \boldsymbol{V}_{\mathbf{bf,P}}}{\mu_{bf}} \tag{14}$$

The steady-state energy equation for two-phase mixture model is defined as;

$$\nabla\nabla.\left(\rho_P\varphi_P\boldsymbol{V}_{\mathbf{P}}h_P + \rho_{bf}\varphi_{bf}\boldsymbol{V}_{\mathbf{bf}}h_{bf}\right) = \nabla.(k_m\nabla T) \tag{15}$$

where, h_{bf} and h_P are known as the enthalpy of base fluid and particles, respectively. Thermal conductivity (k_m) for two-phase mixture model is displayed as follows:

$$k_m = \varphi_{bf}k_{bf} + \varphi_P k_P \tag{16}$$

The volume fraction equation for the two-phase mixture is as below:

$$\nabla.(\varphi_P\rho_P\boldsymbol{V}_{\mathbf{m}}) = -\nabla.(\varphi_P\rho_P\boldsymbol{V}_{\mathbf{dr,P}}) \tag{17}$$

It should be noted that the NF thermo-physical properties are essential parameters in the mixture model.

3.3. Boundary conditions

In single-phase, models, momentum, energy, and continuity equations are calculated with effective NF properties for the problem domain. The simple scheme is employed to solve the velocity pressure coupling. For all equations, a convergence criterion of less than 10^{-6} is used. Boundary conditions of the single-phase model for governing equations are presented with the no-slip condition at the wall;

$$\boldsymbol{u}(R,x) = \boldsymbol{v}(R,x) = 0 \tag{18}$$

and uniform inlet velocity

$$\boldsymbol{u}(r,0) = U, \boldsymbol{v}(r,0) = 0 \tag{19}$$

with constant wall heat flux condition, presented as:

$$q_w^{"} = -K_{eff}\frac{\partial T}{\partial r}|_{r=R} \tag{20}$$

3.4. Thermo-physical properties of the NF

The physical properties of NF play a significant role in the simulation procedure since they strongly affect the computational results. The main problem, however, is related to the classical rules of the mixture that do not apply to the NFs thermal conductivity and dynamic viscosity[42]. Therefore, applying new constitutive models seems to be essential. In the present investigation, experimental correlations are used to determine the thermophysical properties of Al_2O_3-water NF. In addition, the calculation of density and heat capacity of NF are accomplished using mixture models [43,44] as follows:

$$\rho_{nf} = (1-\varphi)\rho_{bf} + \varphi\rho_p \tag{21}$$

$$(\rho\, C_P)_{nf} = (1-\varphi)(\rho\, C_P)_{bf} + \varphi(\rho\, C_P)_p \tag{22}$$

where ρ, ϕ and Cp are the density, the volumetric concentration, and the specific heat, respectively. Subscripts *nf*, *bf*, and *p* indicate NF, base fluid, and NP, respectively. Thermal conductivity derived by Corcione [45] from an experimental study by the variation of Brownian motion, volume concentration, and the NF temperature is expressed as:

$$\frac{K_{nf}}{K_{bf}} = 1 + 4.4Re_p^{0.4}Pr_{bf}^{0.66}\left(\frac{T}{T_{fr}}\right)^{10}\left(\frac{K_p}{K_{bf}}\right)^{0.03}\varphi^{0.66}$$
$$0.2\% \le \varphi \le 9\%, \quad 21 \le T(^\circ C) \le 51, \quad 10\ \text{nm} \le d_p \le 150\ nm \tag{23}$$

where k is the thermal conductivity, Re_p is the NP Reynolds number, T is the NF temperature in Kelvin, T_{fr} is the temperature at the freezing point of the base liquid and Pr is the Prandtl number.

The Reynolds number of the suspended NPs is defined as:

$$Re = \frac{\rho_f \boldsymbol{V}_{\mathbf{Br}} d_p}{\mu_f} = \frac{2\rho_f K_B T}{\pi\mu_f^2 d_p} \tag{24}$$

where V_{Br} is NP Brownian velocity, which is based on the Einstein theory and K_B, is the Boltzmann constant. Hence:

$$\boldsymbol{V_{Br}} = \frac{2K_B T}{\pi\mu_f d_p^2} \tag{25}$$

One of the most common studies for effective viscosity of NF is presented in Eq. (25). The formula is developed by using different experimental data for viscosity as a function of volume fraction, nanoparticles diameter, and temperature as follows [46]:

$$\mu_{nf} = -0.4491 + \frac{28.837}{T} + 0.574\varphi - 0.1634\varphi^2 + 23.053\frac{\varphi^2}{T^2} + 0.0132\varphi^3 - 2354.735\frac{\varphi}{T^3} + 23.498\frac{\varphi^2}{d_p^2} - 3.0185\frac{\varphi^3}{d_p^3} \tag{26}$$
$$1\% \le \varphi \le 9\%, \quad 20 \le T(^\circ C) \le 70, 13\ nm \le d_p \le 131\ nm$$

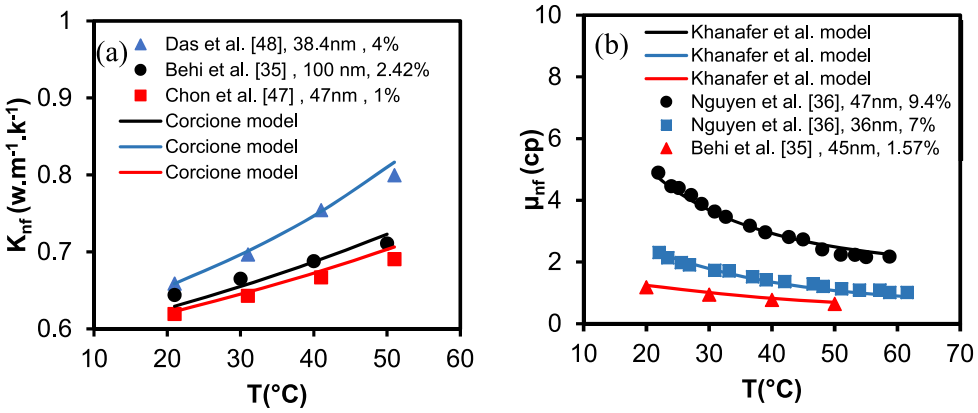

Fig. 3. Models for (a) thermal conductivity and (b) dynamic viscosity as a function of volume fraction, NPs diameter, and temperature and their comparison with experimental results.

Fig. 3a shows the values obtained by the Corcion's model (Eq. (22)) for different volume concentrations and their comparison with some experimental results [35,47,48]. As Fig. 3a displays, estimation of the Corcion's correlation for effective thermal conductivity is in a good agreement with experimental results. In Fig. 3b, the above-described viscosity model has been compared with different experimental results, and according to that, results from this correlation is also in a good agreement with experimental data [35,36].

For selecting appropriate polynomial thermo-physical properties of water, as the base liquid, a simple curve-fitting, which can be observed in the literature [49], was carried out. Corresponding results are presented in Table 1 along with thermo-physical properties of NPs, where the temperature-dependent properties for the solid phase are assumed negligible.

Heat transfer coefficient is calculated by the following formula:

$$h_{nf} = \frac{q''}{T_{w,x} - T_{b,x}} \tag{27}$$

where q'' is constant heat flux on walls, $T_{w,x}$, and $T_{b,x}$ are local wall temperature of the pipe and its bulk temperature, respectively. $T_{w,x}$ is achieved directly from the outputs of the software while T_b should be calculated as below:

$$T_{b,x} = \frac{\int \rho C_P \boldsymbol{V} T dA}{\int \rho C_P \boldsymbol{V} dA} \tag{28}$$

Cp is the fluid specific heat capacity. Accordingly, the average heat transfer coefficient and Nusselt number are computed using equations (29) and (30):

$$h_{av} = \frac{1}{L}\int_0^L h_x dx \tag{29}$$

$$Nu_{av} = \frac{h_{av} D}{K_{nf}} \tag{30}$$

3.5. Numerical methodology and grid-independence study

The computational domain is discretized by a uniform structured grid and exported into Ansys Fluent [50] to solve the governing equations using a finite control volume approach. In order to reach the stable solutions, the second-order central difference is used for estimating diffusion term in the momentum and energy equations and the second-order upwind differencing scheme is used for the convective terms. The mesh independence study carried out, and to ensure the accuracy of numerical results, different numbers of nodes are used in the axial and radial directions. Thus, four different sets of grids are employed in the mesh independency test. For each mesh size, center velocity and Nusselt number were obtained, and the results were compared as displayed in Table 2 and Fig. 4. It is evident that the results of meshes 4000 × 8 and 5000 × 10 are very close and it indicates that the mesh independence is achieved by M3. Thus, it was selected for all the simulations in this paper.

4. Results and discussion

4.1. Experimental results

In this section, an experiment conducted with water-based nanofluid containing Al_2O_3 nanoparticles for both convective heat transfer and friction factor. The local nusselt number of nanofluids in the laminar flow for Re = 915, Pr = 5.06 at constant heat flux is

Table 1
Thermophysical properties of water and NPs.

	P (kg/m^3)	Cp (J/kg.K)	K (W/m.K)	μ (kg/m.s)
Al_2O_3	3970	765	27	–
Water	$765.33 + 1.8142 \times T - 0.0035 \times T^2$	$(28.7 - 0.2817 \times T + 0.00125 \times T^2 - 2.48e^{-6} \times T^3 + 1.857e^{-9} \times T^4) \times 1000$	$-0.5752 + 0.006397 \times T - 8.151e^{-6} \times T^2$	$0.0967 - 8.207e^{-4} \times T + 2.344e^{-6} \times T^2 - 2.244e^{-9} \times T^3$

Table 2
Comparison of the average Nusselt number for four different mesh sizes.

Mesh sizes	5000 × 10:M4	4000 × 8:M3	3000 × 6: M2	2000 × 4: M1
Nu_{ave}	4.71	4.73	4.79	4.93

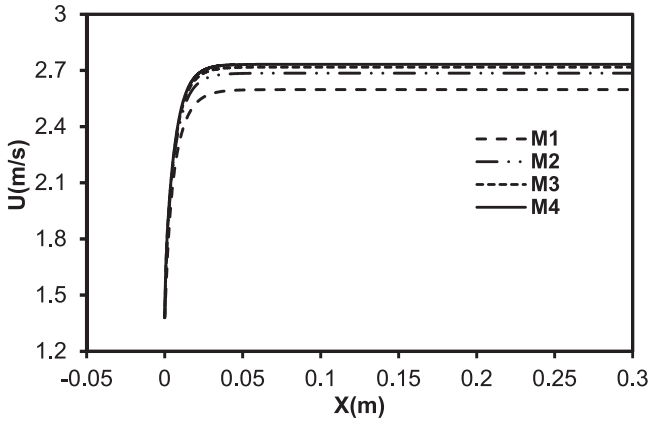

Fig. 4. Comparison of flow velocity in centerline for four different mesh sizes for Re = 913.

shown in Fig. 5. The model is validated by comparing the numerical results of pure water as base liquid with the theoretical and experimental data. Fig. 5a and b shows the obtained result of the Nusselt number and friction factor in the fully developed laminar flow of pure water and their comparison with Shah's correlations where itis defined as [51]:

$$Nu_x = \begin{cases} \dfrac{1.302}{(Gz)^{\frac{1}{3}}} - 1 & 1/Gz \le 0.00005 \\ \dfrac{1.302}{(Gz)^{\frac{1}{3}}} - 0.5 & 0.0005 \le 1/Gz \le 0.0015 \\ 4.364 + \dfrac{8.68}{(1000Gz)^{0.506} e^{-\frac{41}{Gz}}} & 1/Gz \ge 0.0015 \end{cases} \quad (31)$$

Graetz number (RREFERNCE) is defined as:

$$Gz = \frac{D}{x} RePr \quad (32)$$

As can be observed in Fig. 5, a good agreement exists between the numerical and experimental results with theoretical correlations validating the present numerical simulation. Computational results show that there is less than a 10% error between numerical results for the Nusselt number and friction factor with theoretical and experimental data.

The hydrothermal performance of NFs was studied in a wide range of Re number from 400 to 2180 where the NP size and loading vary from 13 nm to 130 nm and 0 to 9 vol%, respectively. Fig. 6 illustrates the heat transfer coefficient versus axial distance from inlet achieved and its comparison with experimental investigation accomplished by Rea et al. [52]. A good agreement is observed between experimental data [52] and numerical results.

In the present study, there is a very good agreement between the results achieved from models and the experimental data, within a relative error range of 8%. In particular, the agreement between numerical and experimental results of the thermophysical properties of NF is crucial for obtaining more reliable results in the NFs hydrothermal simulation. The effect of various parameters including the size of the particle, volume concertation, Re number, and *Pe* number on laminar fluid flow and heat transfer

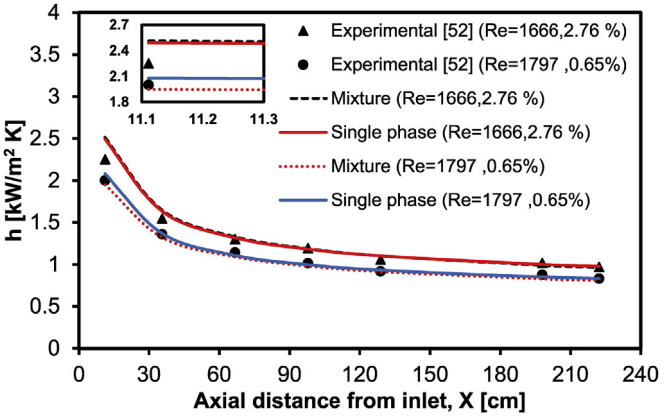

Fig. 6. Comparison of heat transfer coefficient of different numerical simulations with the experimental results for the various axial distance from the inlet.

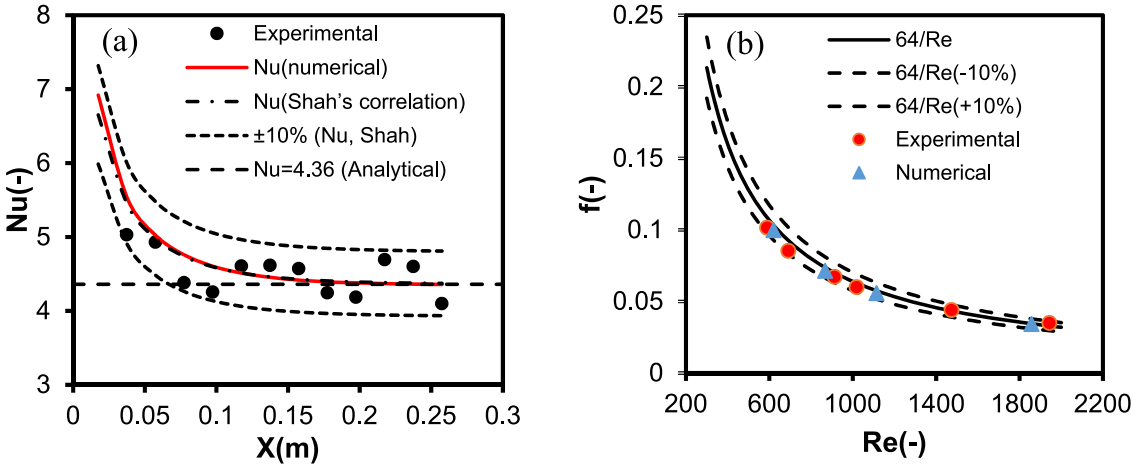

Fig. 5. (a) Local Nusselt number conventional fluid in the laminar flow for Re = 915, Pr = 5.06 at constant heat flux; (b) Comparison of friction factor of the present numerical computations with the theoretical and experimental results for various Reynolds numbers.

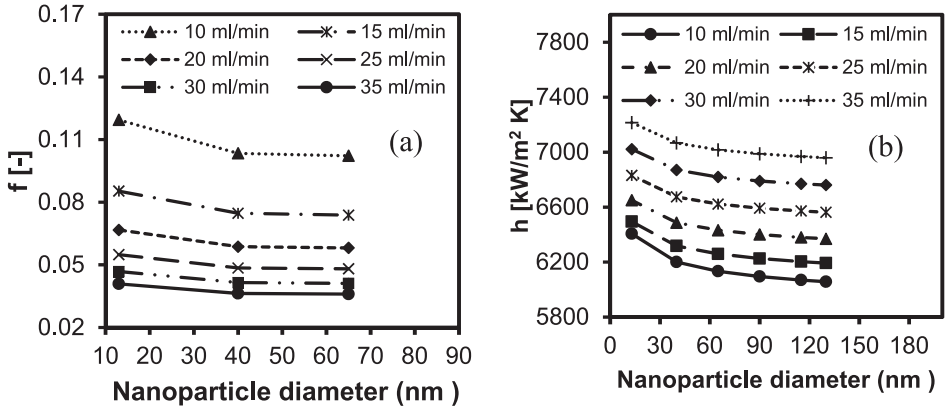

Fig. 7. a) Change in friction factor versus the size of nanoparticle at the volume concentration of 1% b) Change in average heat transfer coefficient versus the size of nanoparticle at a volume concentration of 1%.

of Al_2O_3 NF in a uniform microtube, are presented. Furthermore, we did not observe a significant difference between the single and two-phase modeling results.

Fig. 7(a) and (b) depict the change in friction factor and average heat transfer coefficient of the NF in different diameters of nanoparticles for different volume flow rates at the inlet of the microtube. The heat transfer coefficient increases by the increase in volume flow rate, whereas the friction factor decreases. In addition, the increase in volume flow rate leads to the rise in kinetic energy. Consequently, dynamic pressure, which is included in an inverse correlation with friction factor, increases. Thus, it decreases the friction factor. Furthermore, the volume flow rate increment raises the proportion of convective heat transfer to conductive heat transfer. It could be concluded from this investigation that the nanofluids with smaller particles have a higher effective heat transfer and as a result heat transfer coefficient. As shown in Fig. 7(a), the size of nanoparticles influences the friction factor, particularly in the smaller size range while for nanofluids with containing nanoparticles over 40 nm this effect is negligible. Another observation is that the nanoparticle size has more effect on the friction factor in lower volume flowrates compared to 30 ml/min and above. Dispersing relatively smaller nanoparticles increase the contact surface, viscosity and Brownian motion of the particle that all of these phenomena result in falling the friction factor, mainly in lower velocity (volume flow rates).

Fig. 8(a) shows that pressure drop in microtube for water and NF for different NP loadings. Based on that NF exhibits a higher pressure drop than pure water as the base liquid. As it is elucidated in Fig. 8(a), pressure drop grows with the rise in Re number. NPs dispersed in a coolant remarkably raise pressure drop due to their higher viscosity.

Pumping power for water and NF in microtube at different volume concentrations and Re numbers are compared in Fig. 8(b). It can be observed that due to the presence of NPs and an increase in their volume concentration in fluid, dynamic viscosity and density are increased. Since more viscous fluid requires more pumping power to move in a microchannel, measured pumping power for such fluids raises, as shown in Fig. 8(b). By an increase in Re number or velocity, in other words, higher pumping power is required as well because of the higher volume flow rate.

Hydrothermal performance of NF with diameter from 13 to 90 nm is evaluated. Change in heat transfer coefficient relative to pumping power using equation (33) is illustrated in Fig. 9.

$$P_{nf} = \frac{\dot{m}_{nf}\Delta P}{\rho_{nf}} \tag{33}$$

Fig. 9(a) shows that as volume concentration of NFs increases, the average heat transfer coefficient and pumping power are growing. This behavior more obvious while smaller NPs are employed. In Fig. 9(b), average heat transfer coefficient for NFs with a diameter of particles varying from 13 to 90 nm, and volume

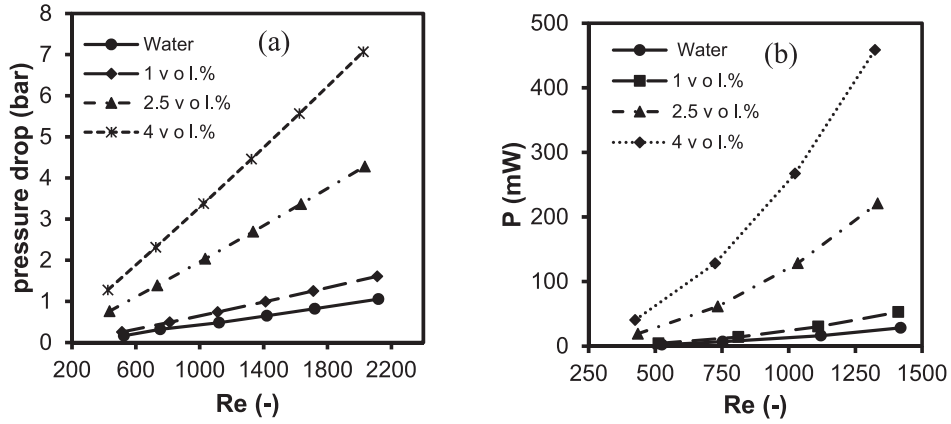

Fig. 8. a) Change in pressure drop in different Re numbers for Al_2O_3 NPs with a diameter of 13 nm b) Comparison of water-based NF pumping power at various Re numbers and volume concentrations at a diameter of 13 nm.

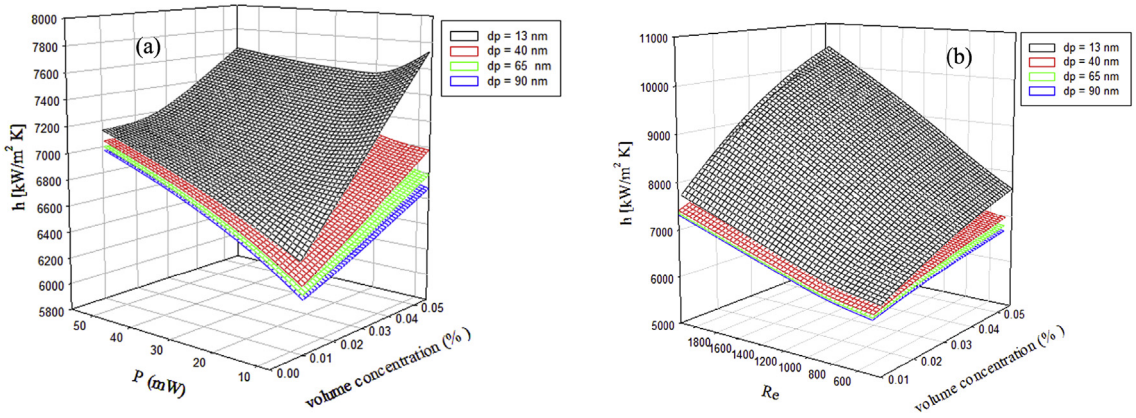

Fig. 9. Hydrothermal performance (Average heat transfer coefficient) of NFs at different NP sizes, (a) function of volume concentration and pumping power (b) effect of Re number and nanoparticle loading.

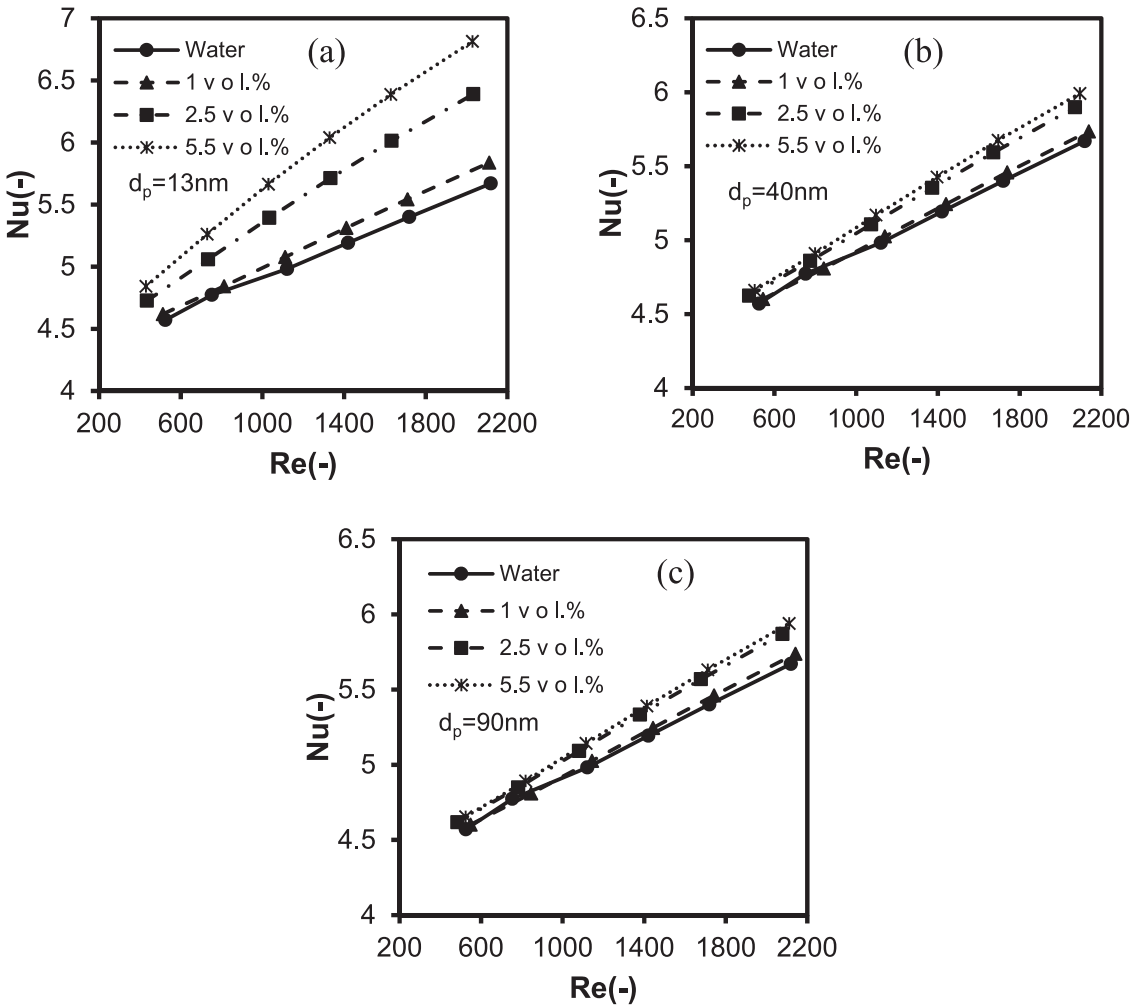

Fig. 10. Effect of Re number on the average Nusselt number of water and NF at different concentrations and the particle diameter of (a) 13 nm (b) 40 nm (c) 90 nm.

concentration from 1% to 5.5% at different Re numbers are shown. As it has been depicted, the average heat transfer coefficient increases by growing Re number and concentration of NPs.

In the next part, the average Nusselt number is also evaluated for water and NF at various concentrations (1%, 2.5%, and 5.5%), particle diameters (13, 40, and 90 nm) and Re numbers. It was found that by decreasing the particle diameter and increasing the concentration, at constant Re number, Nusselt number raises, as shown in Fig. 10(a)–(c). Moreover, at a constant concentration, an increase in Re number causes a higher average Nusselt number. As

expected, when both concentration and Re number are increased, higher Nusselt numbers are obtained. The reason for the increase in Nusselt number at higher volume concentrations of NFs compared to pure water is the presence of nanoparticle in the base liquid that grows thermal conductivity of NFs and as a result, improves heat transfer performance.

Considering Figs. 9 and 10, by reducing the particle diameters, the specific area is increased, and this phenomenon may cause more Brownian motion and improvement of the heat transfer performance. Besides, nanoparticles with the higher specific area are in contact with more molecules from the base liquid that it may results in better heat transfer performance of NF together with an increase in heat transfer coefficient and Nusselt number. Finally, the impact of particle concentration decreases by an increase in the size of nanoparticles. In other words, as the size of particles is getting bigger, dispersing nanoparticles in base fluids has less effect on the Nusselt number. Thus, it could be concluded that the bigger the size of nanoparticles, this declining trend is more evident, as shown in Figs. 8 and 10(c).

To evaluate the effect of NP size on the average Nusselt number, change in Nusselt number concerning *Pe* number for different diameters of Al_2O_3 are presented in Fig. 11. *Pe* number represents the

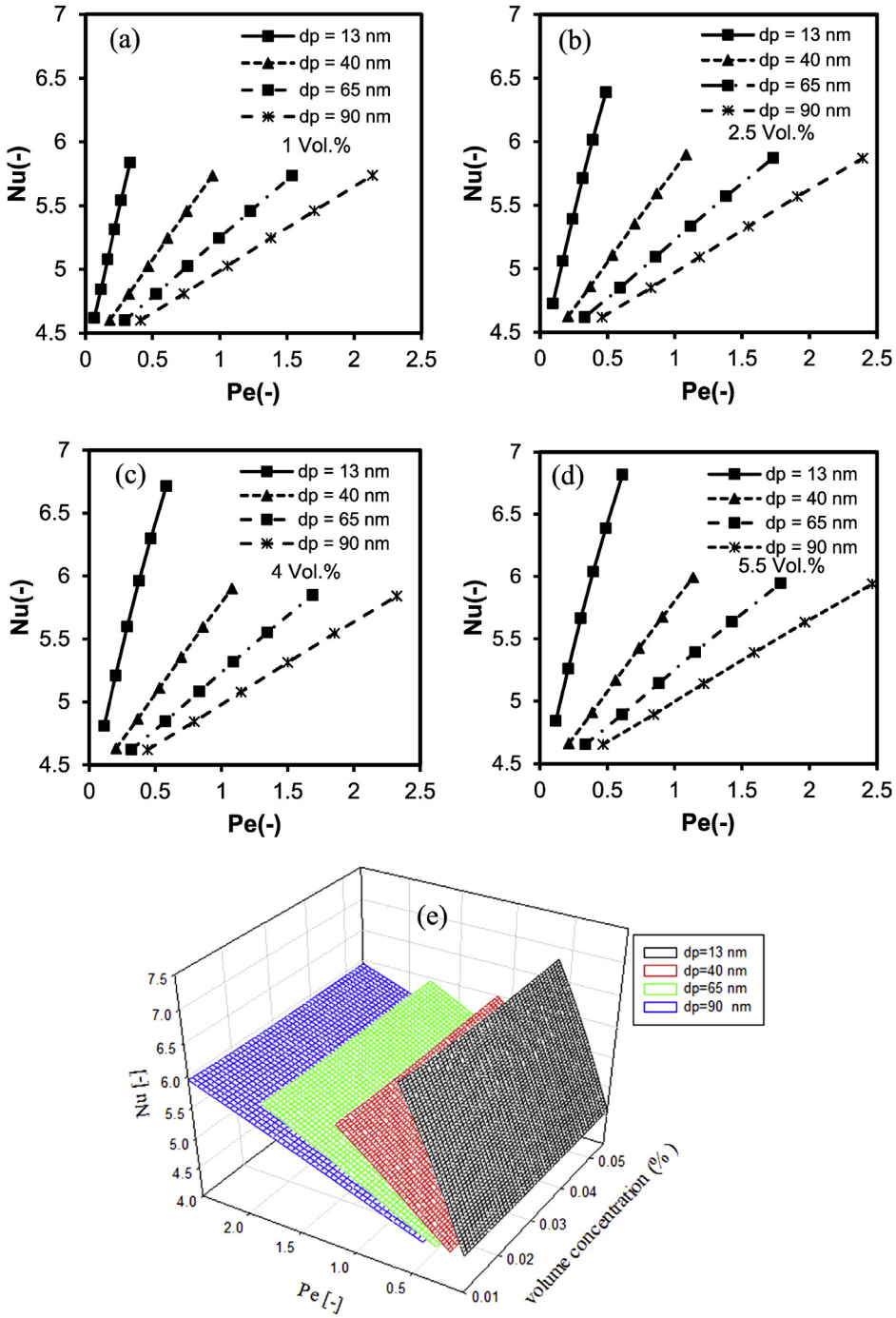

Fig. 11. Average Nusselt number of NF at different sizes of NPs versus *Pe* number, (a) 1 vol% (b) 2.5 vol% (c) 4 vol% (d) 5.5 vol%, and (e) various *Pe* numbers and NP volume concentrations.

effect of the adjective transfer rate and micro-diffusion of NFs. At constant volume concentration, the average Nusselt number raises by using smaller particles. When the size of NPs is decreased, Brownian motion and a random number of NPs are increased resulted in improving the heat transfer performance of NFs. Higher Nusselt numbers are observed at higher concentrations with smaller particle sizes. For instance, Fig. 11(a) illustrates that at concentration of 1% and *Pe* number of 0.3, when particle's diameter changes from 13 nm to 65 nm, the average Nusselt number decreases from 5.84 to 4.6. Similar behaviors could be observed in Fig. 11(b)–(d), similarly in Fig. 11(e) in the form of a contour plot.

Fig. 12 represents a change in the average heat transfer coefficient of NF with respect to change in concentration and particle size of NF. This part of the study is accomplished for NP's diameters of 13 nm, 40 nm, 65 nm, 90 nm, 115 nm, and 130 nm as well as the concentrations of 1%, 2.5%, 4%, 5.5%, 7%, and 9%. On one hand, by increasing the NP volume concentration, a more significant number of particles are involved in improving the heat transfer performance. On the other hand, at the constant NP volume concentration, an increase in the number of particles causes for deduction of Brownian motion and specific area that all of them result in a lower heat transfer coefficient.

Overall, in the NP concentration range of 1%–9% and NP size range of 13–130 nm, we observed that the suspended NPs remarkably increased the convective heat transfer coefficient as well as friction factor compared to that of ultra-pure water. Larger viscosities are expected for the higher nanoparticle loading resulting in higher pressure losses and friction factors. The friction factor of 9 wt% nanofluid has an increase of about 22%, implying the penalty for pressure drop in the case of nanofluids with higher concentrations. In addition, the maximum improvement of the convective heat transfer coefficient was about 42% for a concentration of 0.9 wt% of nanoparticles. Thus, from the thermal performance standpoint of view, the utilization of nanofluid would in the laminar regime be advantageous.

4.2. Correlations for the nusselt number and friction factor

It has been observed that Nusselt number, Re number, *Pe* number, and Pr number are dependent on thermo-physical properties including ρ, μ, k, and C_p that vary by a change in particle concentration and size of the nanoparticle. Also, the studied parameters, i.e., friction factor and heat transfer coefficient, are dependent on all the parameters mentioned above. Based on results from the previous section as well as data depicted in Fig. 13(a) and (b), both heat transfer coefficient and friction factor change as concentration and size of NP vary. Consequently, the Nusselt number is a function of Re number, Pr number, *Pe* number, and volume concentration.

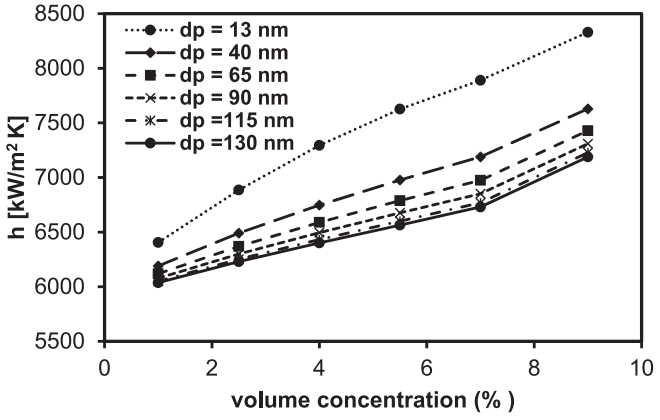

Fig. 12. Average heat transfer coefficient versus volume concentrations at different sizes of particles.

Numerical simulations are conducted in the fully developed hydraulic and thermal region, and 222 data points are collected. Then, Minitab statistical software [53] are applied to develop a new correlation (Equation (34)). The new correlation is an optimized correlation already proposed by Xuan and Li [37], and it is valid for volume concentrations below 9%, Re numbers between 400 and 2180, *Pe* number smaller than 8.59, and Pr number between 4.15 and 16.15. When the volume concentration is zero, the results for pure water are achieved.

The new correlation is in good agreement with numerical data, and the maximum deviation is ±8%, as shown in Fig. 14.

$$Nu = 1.119\left(1 + 0.1859\phi^{0.754}Pe_p^{0.218}\right)Re_{nf}^{0.1716}Pr_{nf}^{0.1786}$$
$$400 < Re_{nf} < 2180, 4.15 < pr_{nf} < 16.15, 0 < pe_p < 8.59, \phi < 0.09 \quad (34)$$

Following the similar approach as above, a new correlation (Equation (35)) is developed for friction factor at the fully developed hydraulic region. In this correlation, a variation of the friction factor at different Re numbers, volume concentration, and sizes of NP are considered. When the volume concentration is zero, the results for pure water are achieved. The new correlation is in good agreement with numerical data, and the maximum deviation is ±5%, as shown in Fig. 15. It is valid under the conditions below:

$$400 < Re_{nf} < 2180, \frac{d_P}{D} < 0.00026, \ \phi < 0.09$$
$$f = 55.36Re_{nf}^{-0.9826}\left(1 + \varphi\frac{d}{D}\right)^{4.835} \quad (35)$$

5. Conclusion

In this study, laminar single-phase fluid flow and convective heat transfer performance of NF in a circular microtube under the constant wall temperature condition in a fully developed region was investigated. All thermo-physical properties of NF including density, specific heat capacity, thermal conductivity, and dynamic viscosity to calculate the heat transfer coefficient and friction factor up to 9 vol% and size of NP from 13 to 130 nm are computed based on the existing correlations. Two correlations were proposed to predict heat transfer coefficient and friction factor at specific volume concentration and size of NP in the thermally developing and hydrodynamic developed regions. Brief descriptions of results from the numerical simulation are indicated below:

- Dispersing NPs in a base liquid increases heat transfer performance as well as the viscosity of the NFs. Furthermore, the increase in volume concentration and a decrease in the size of NPs improve heat transfer performance and viscosity of the NFs.
- Re number has a significant impact on the heat transfer coefficient, and Nusselt number as greater Re number causes for the higher Nusselt number. At a constant Re number, Nusselt number of a NF is higher than that of the base liquid. It should be noted that the temperature of NF in the vicinity of the wall is less than that of base liquid.
- The heat transfer coefficient and Nusselt number of NFs are higher than the base liquid. An increase in the volume

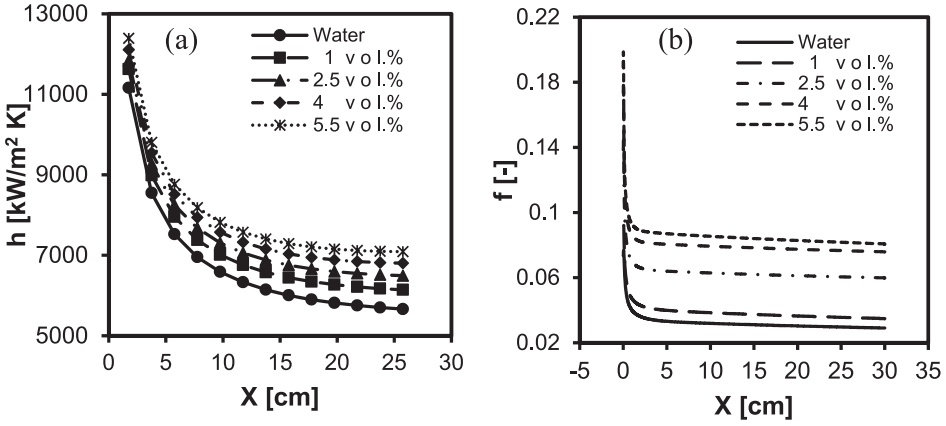

Fig. 13. a) Local heat transfer coefficient, b) Friction factor, versus axial distance from the inlet at different NP volume concentrations and its diameter of 13 nm.

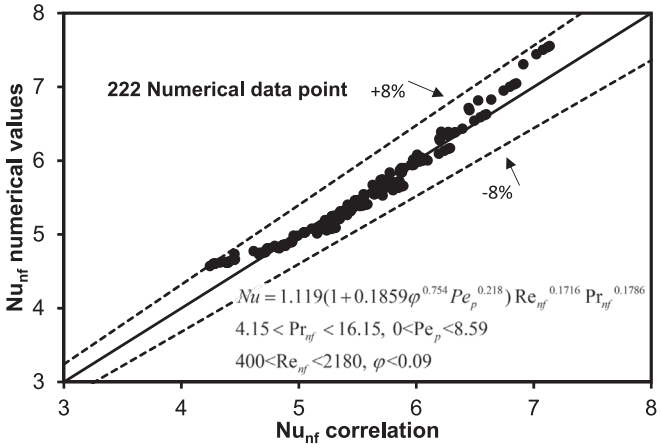

Fig. 14. Comparison between Nusselt numbers achieved from presented correlation (Equation (34)) with Nusselt numbers obtained from the numerical study.

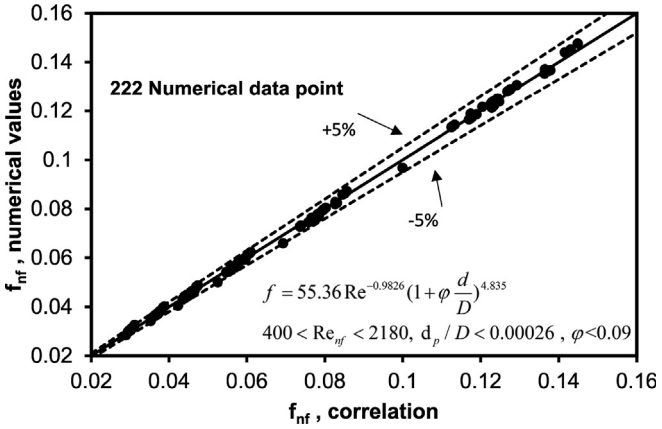

Fig. 15. Comparison between friction factors achieved from presented correlation (Equation (35)) with friction factors obtained from the numerical study.

concentration and decrease in the size of NP lead to the higher value of the heat transfer coefficient and consequently Nusselt number.

- The friction factor of NFs is higher than the base liquid. An increase in the volume concentration and a decrease in the size of NP results in a higher value of pumping power as well.
- The correlations were developed to predict the Nusselt number and friction factor of NFs, with ±8% and ±5% agreement and between numerical data and predictions, respectively.

Acknowledgment

The financial supports from International Postgraduate Research Scholarships (IPRS) at The University of Sydney, the EU (Project Reference: 228882) and the KTH-Royal Institute of Technology are highly appreciated.

References

[1] Karniadakis G, Beskok A, Aluru N. Microflows and Nanoflows: Fundamentals and Simulation. 2005. p. 123. Cited on.
[2] Kim M, Ha D, Kim T. Cracking-assisted photolithography for mixed-scale patterning and nanofluidic applications. Nat Commun 2015;6.
[3] Murshed SMS, Leong KC, Yang C. Enhanced thermal conductivity of TiO2—-water based nanofluids. Int J Therm Sci 2005;44(4):367–73.
[4] Zhang Y. Nano/microscale heat transfer. 2007.
[5] Haghighi EB, et al. Cooling performance of nanofluids in a small diameter tube. Exp Therm Fluid Sci 2013;49(0):114–22.
[6] Lemmon EW, Jacobsen RT. Viscosity and thermal conductivity equations for nitrogen, oxygen, argon, and air. Int J Thermophys 2004;25(1):21–69.
[7] Vo TQ, Kim B. Transport phenomena of water in molecular fluidic channels. Sci Rep 2016;6:33881.
[8] Javanmardi M, Jafarpur K. A molecular dynamics simulation for thermal conductivity evaluation of carbon nanotube-water nanofluids. J Heat Transf 2013;135(4):042401.
[9] Mirmohammadi SA, et al. Particle-shape-, temperature-, and concentration-dependent thermal conductivity and viscosity of nanofluids. Phys Rev 2019;99(4):043109.
[10] Choi SU, Eastman JA. Enhancing Thermal Conductivity of Fluids with Nanoparticles. IL (United States): Argonne National Lab.; 1995.
[11] Eastman JA, et al. Anomalously increased effective thermal conductivities of ethylene glycol-based nanofluids containing copper nanoparticles. Appl Phys Lett 2001;78(6):718–20.
[12] Lee S, Choi SU-S. Application of Metallic Nanoparticle Suspensions in Advanced Cooling Systems. IL (United States): Argonne National Lab.; 1996.
[13] Das SK. Nanofluids—the cooling medium of the future. Heat Transf Eng 2006;27(10):1–2.
[14] Wang X-Q, Mujumdar AS. A review on nanofluids-part II: experiments and applications. Braz J Chem Eng 2008;25(4):631–48.
[15] Yener Y, et al. Single-phase forced convection in microchannels. In: Microscale Heat Transfer Fundamentals and Applications. Springer; 2005. p. 1–24.
[16] Shah R, London A. Thermal boundary conditions and some solutions for laminar duct flow forced convection. J Heat Transf 1974;96(2):159–65.
[17] Buongiorno J, Hu LW. Nanofluid Heat Transfer Enhancement for Nuclear Reactor Applications. 2009.
[18] Barrett TR, et al. Investigating the use of nanofluids to improve high heat flux cooling systems. Fusion Eng Des 2013;88(9–10):2594–7.
[19] Buongiorno J. Convective transport in nanofluids. J Heat Transf 2006;128(3):240–50.
[20] Das SK, Choi SU, Patel HE. Heat transfer in nanofluids—a review. Heat Transf Eng 2006;27(10):3–19.
[21] Wang XQ, Mujumdar AS. Heat transfer characteristics of nanofluids: a review.

Int J Therm Sci 2007;46(1):1–19.
[22] Hwang KS, Jang SP, Choi SU. Flow and convective heat transfer characteristics of water-based Al 2 O 3 nanofluids in fully developed laminar flow regime. Int J Heat Mass Transf 2009;52(1):193–9.
[23] Hojati M, et al. Convection heat transfer of non-Newtonian nanofluid through a uniformly circular tube. Exp Therm Fluid Sci 2011;35:1351–6.
[24] Haghighi EB, et al. Screening single phase laminar convective heat transfer of nanofluids in a micro-tube. In: Journal of Physics: Conference Series. IOP Publishing; 2012.
[25] Nguyen C, et al. Heat Transfer Enhancement by Using Nanofluids for Cooling of High Heat Output Microprocessor. TechBrief: Electronics Cooling; 2007. p. 1–4.
[26] Koo J, Kleinstreuer C. Laminar nanofluid flow in microheat-sinks. Int J Heat Mass Transf 2005;48(13):2652–61.
[27] Lee J, Mudawar I. Assessment of the effectiveness of nanofluids for single-phase and two-phase heat transfer in micro-channels. Int J Heat Mass Transf 2007;50(3):452–63.
[28] Ganesan P, et al. Turbulent forced convection of Cu–water nanofluid in a heated tube: improvement of the two-phase model. Numer Heat Transf, Part A: Appl 2016;69(4):401–20.
[29] Hung YM. Analytical study on forced convection of nanofluids with viscous dissipation in microchannels. Heat Transf Eng 2010;31(14):1184–92.
[30] Lelea D, Nisulescu C. The micro-tube heat transfer and fluid flow of water based Al2O3 nanofluid with viscous dissipation. Int Commun Heat Mass Transf 2011;38(6):704–10.
[31] Azizi Z, Alamdari A, Malayeri M. Thermal performance and friction factor of a cylindrical microchannel heat sink cooled by Cu-water nanofluid. Appl Therm Eng 2016;99:970–8.
[32] Zhang H, et al. Heat transfer and flow features of Al2O3–water nanofluids flowing through a circular microchannel – experimental results and correlations. Appl Therm Eng 2013;61(2):86–92.
[33] S I, et al. Investigation on convective heat transfer and friction factor of silver–water nanofluid under laminar flow – an experimental study. Heat Mass Transf 2019;55(10):3029–39.
[34] Keshavarz Moraveji M, et al. Numerical evaluation on thermal–hydraulic characteristics of dilute heat-dissipating nanofluids flow in microchannels. J Therm Anal Calorim 2019;135(1):671–83.
[35] Behi M, Mirmohammadi SA. Investigation on Thermal Conductivity, Viscosity and Stability of Nanofluids. Stockholm, Sweden: Royal Institute of Technology (KTH) School of Industrial Engineering and Management; 2012.
[36] Nguyen C, et al. Temperature and particle-size dependent viscosity data for water-based nanofluids–hysteresis phenomenon. Int J Heat Fluid Flow 2007;28(6):1492–506.
[37] Li Q, Xuan Y, Wang J. Investigation on convective heat transfer and flow features of nanofluids. J Heat Transf 2003;125:151–5. 2003.
[38] Naumann Z, Schiller L. A drag coefficient correlation. Z Ver Deutsch Ing 1935;77:318–23.
[39] Andraos J. On the propagation of statistical errors for a function of several variables. J Chem Educ 1996;73(2):150.
[40] Bahiraei M. A comprehensive review on different numerical approaches for simulation in nanofluids: traditional and novel techniques. J Dispersion Sci Technol 2014;35(7):984–96.
[41] Manninen M, Taivassalo V, Kallio S. On the mixture model for multiphase flow. Technical Research Centre of Finland Finland; 1996.
[42] Aybar HŞ, et al. A review of thermal conductivity models for nanofluids. Heat Transf Eng 2014;36(13):1085–110.
[43] Drew DA, Passman SL. Theory of multicomponent fluids, vol. 135. Springer Science & Business Media; 2006.
[44] Xuan Y, Roetzel W. Conceptions for heat transfer correlation of nanofluids. Int J Heat Mass Transf 2000;43(19):3701–7.
[45] Corcione M. Empirical correlating equations for predicting the effective thermal conductivity and dynamic viscosity of nanofluids. Energy Convers Manag 2011;52(1):789–93.
[46] Khanafer K, Vafai K. A critical synthesis of thermophysical characteristics of nanofluids. Int J Heat Mass Transf 2011;54(19):4410–28.
[47] Chon CH, et al. Empirical correlation finding the role of temperature and particle size for nanofluid (Al 2 O 3) thermal conductivity enhancement. Appl Phys Lett 2005;87(15). 153107-153107-3.
[48] Das SK, et al. Temperature dependence of thermal conductivity enhancement for nanofluids. J Heat Transf 2003;125(4):567–74.
[49] McNab G, Meisen A. Thermophoresis in liquids. J Colloid Interface Sci 1973;44(2):339–46.
[50] Ver, A.F., Software Package. Ansys Fluent Inc., Canonsburg, PA, USA.
[51] Shah RK, London AL. Laminar Flow Forced Convection In Ducts: A Source Book For Compact Heat Exchanger Analytical Data. Academic press; 2014.
[52] Rea U, et al. Laminar convective heat transfer and viscous pressure loss of alumina–water and zirconia–water nanofluids. Int J Heat Mass Transf 2009;52(7–8):2042–8.
[53] Minitab I. Minitab 17 Statistical Software [Computer Software]. 2010 [State College, PA].